Assessment of peak tsunami amplitude associated with a great earthquake occurring along the southernmost Ryukyu subduction zone for Taiwan region

Yu-Sheng Sun[1], Po-Fei Chen[1], Chien-Chih Chen[1], Ya-Ting Lee[1], Kuo-Fong Ma[1] and Tso-Ren Wu[2]

5   [1]Department of Earth Sciences, National Central University, Taoyuan City, Taiwan 320, R.O.C.
[2]Graduate Institute of Hydrological and Oceanic Sciences, National Central University, Taoyuan City, Taiwan 320, R.O.C.

Correspondence to: Yu-Sheng Sun (shengfantasy@gmail.com)

Abstract. The southernmost portion of the Ryukyu Trench closed to Taiwan island is a potential region to generate 7.5 to 8.7 tsunami earthquakes by shallow rupture. The fault model for this potential region dips 10° northward with rupture length of

10   120 km and width of 70 km. The earthquake magnitude estimated by fault geometry is Mw 8.15 with 8.25 m average slip as a constrain of earthquake scenario. The heterogeneous slip distributions over rupture surface are generated by stochastic slip model, the slip spectrum with k^{-2} decay in wave number domain, and they are consistent with above identical seismic conditions. The results from tsunami simulation illustrate that the propagation of tsunami waves and the peak wave heights largely vary in response to the slip distribution. The wave phase changing is possible as the waves propagate, even under the same seismic

15   conditions. The tsunami energy path is not only following the bathymetry but also depending on slip distribution. The probabilistic distributions of peak tsunami amplitude calculated by 100 different slip patterns from 30 recording stations reveal the uncertainty decreases with distance from tsunami source. The highest wave amplitude for 30 recording points is 7.32 m at Hualien for 100 different slips. Comparing with stochastic slips, uniform slip distribution will be extremely underestimated, especially in near field. In general, uniform slip assumption only represents the average phenomenon so that it will ignore

20   possibility of tsunami wave. These results indicate that considering effect of heterogeneous slip distribution is necessary for assessing tsunami hazard and that can provide more information about tsunami uncertainty for a more comprehensive estimation.

1 Introduction

Almost all destructive tsunamis are generated by shallow earthquakes that occur at subduction zone. There are recently

25   destructive tsunami events: the 2004, Mw 9.1, Sumatra earthquake (Lay et al., 2005), the 2010, Mw 8.8, Chile earthquake (Lay et al., 2010; Fritz et al., 2011) and the 2011, Mw 9.0, Tohoku earthquake (Goda et al., 2015; Goda and Song, 2016) and all of them occurred at subduction zone. The island of Taiwan located at the convergent boundary between the Philippine Sea Plate and the Eurasian Plate is possibly threatened from tsunami. The convergence rate in this area is approximately 80-85 mm/yr (Seno et al., 1993; Yu et al., 1997; Sella et al., 2002; Hsu et al., 2009; Hsu et al., 2012). Thus, earthquakes occur frequently in

and around Taiwan. The shallow earthquakes that occur in the Manila Trench to the south and the Ryukyu Trench to the northeast are particularly tsunamigenic Also, the earthquakes in southernmost Ryukyu Trench is more active than north Manila Trench (Wu et al., 2013). The most well-known historic tsunami events that have occurred in northeast Taiwan are the 1867 Keelung earthquake (Mw 7.0) (Tsai 1985; Ma and Lee, 1997; Cheng et al., 2016; Yu et al., 2016) and the 1771 Yaeyama

5 (Japan) earthquake (M_w~8) (Nakamura, 2009a). The historic recording demonstrates that Taiwan island has the potential of tsunami threat. Furthermore, the 2011 Tohoku earthquake induced powerful tsunami that destroyed coastal areas and caused nuclear accidents (Mimura et al., 2011). There are four nuclear power plants along the coast on Taiwan island so that it is necessary to carefully estimate the tsunami hazard and compound disasters.

10 Probabilistic tsunami hazard analysis (PTHA) is a modification of probabilistic seismic hazard analysis (PSHA) (Cornell, 1968; SSHAC, 1997), and it is intended to forecast as comprehensively as possible the probability of tsunami hazards for a given region. Considering tsunamis triggered by earthquakes, the recurrence rates of earthquakes have typically been estimated using the Gutenberg–Richter relationship (Gutenberg and Richter, 1944) for a defined source region. The assessment of wave heights is one of the primary differences between PTHA and PSHA. PSHA assesses ground motion based on empirical attenuation

15 relationships (Wang et al., 2016). PTHA assesses tsunami wave heights using empirical approaches or tsunami simulations (Geist, 2002; Geist and Parsons, 2006; Geist and Parsons, 2009). Geist and Parsons (2006) mentions that the tsunami wave height follows a definable frequency-size distribution over a sufficiently long amount of time at a given coastal region (Soloviev, 1969; Houston et al., 1977; Horikawa and Shuto, 1983; Burroughs and Tebbens, 2005). This method is of great use in establishing tsunami probability for regions if there is an extensive catalog of observed tsunami wave heights. Given the

20 wide distribution of global tsunamigenic earthquakes within seafloor regions at subduction zones, the tsunami records obtained from coastal gauges or/and ocean buoys are too sparse to assess the associated hazards comprehensively, and the recording time since their deployment is too short to enable study of the recurrence intervals of tsunamis/earthquakes. The existing tsunami catalogue is limited so that the simulation is an effective approach. Conventional tsunami simulation adopts simple source approximation and applies elastic dislocation theory to calculate the deformation of the seafloor surface assuming a

25 uniform slip over entire fault surface (Okada, 1985; Okal, 1982). However, the complexity of earthquake ruptures plays a substantial role in tsunami generation. Conventional approaches are therefore unable to capture various features of short-wavelength tsunamis in the near field (Geist, 2002; Geist and Parsons, 2009). Previous studies that simulate tsunamis resulting from historical earthquakes around Taiwan (Ma and Lee, 1997; Wu et al., 2008) using uniform slip models agree only with long-wavelength observations. For hazard mitigation, it is critical that the amplitudes of tsunamis are predicted along various

30 coasts for a given earthquake as accurately as possible. To make such predictions, the effects of rupture complexity must be taken into consideration. Recent developments in PTHA have included the adoption of stochastic slip distributions of earthquakes to determine the overall probability of particular tsunami heights. (Geist and Parsons, 2006, 2009). That method can be able to quantify the variations for a reasonable estimation in evaluating the probability of specified tsunami heights at individual locations that result from a specific fault.

In this study, we assess tsunami heights along the coasts of Taiwan that is caused by the potential tsunamigenic zone at the southernmost end of the Ryukyu subduction zone. This potential zone is close to Taiwan and at least ten earthquakes ($M_w>7$) have occurred over the past 100 years (Hsu et al., 2012). The largest one is Mw 7.7 in 1920 (Theunissen et al., 2010). For this area, the plausible magnitude of greatest earthquake was determined to a range between 7.5 and 8.7 (M_w) (Hsu et al., 2012). The fault zone is bounded by the Longitudinal Valley Fault to the west and the Gagua Ridge to the east (Hsu et al., 2012). This defined fault geometry with rupture length and width was employed and earthquake with magnitude 8.15 is used in the tsunami simulations. The stochastic slip model is invoked to describe the uncertainty of the rupture pattern over the fault plane to enable a more realistic assessment of tsunami probability.

2 Great earthquake scenario and tsunami simulation

2.1 Assessment of Seismic Parameters

The estimating magnitude of the maximum possible earthquake scenario is essential for the fundamental seismic condition of tsunami simulation. This scenario, potential rupture fault, proposed by Hsu et al. (2012) occurs along the southernmost Ryukyu trench with rupture length of 120 km, width of 70 km and dip of 10° and extends to a depth of 13 km. Kanamori and Anderson (1975) investigated the relation between rupture area and moment, which revealed that the most average stress drops ($\Delta\sigma$) between 10 to 100 bars. The average stress drops for the most interplate earthquakes are around 30 bars so that we set an average stress drop of 30 bars. According to the stress drop and seismic moment (M_0) relations in dip slip faults (Kanamori and Anderson, 1975):

$$M_0 = \frac{\pi(\lambda+2\mu)}{4(\lambda+\mu)}\Delta\sigma W^2 L \tag{1}$$

W and L is width and length of rupture plane respectively. We can obtain the moment for this scenario under the average stress drop of 30 bars and with a definite rupture geometry. In Eq. (1), μ is rigidity and λ is the Lamè parameter. We assume that the crust is elastic and homogeneous. Hence, $\mu = \lambda = 30$ GPa (Fowler, 2004; Piombo et al, 2007). Additionally, the seismic moment can be presented by rupture area and average slip as below (Lay and Wallace, 1995):

$$M_0 = \mu A \overline{D} \tag{2}$$

The seismic moment, moreover, is dependent on rupture area (A) and average slip ($\overline{D}$) so that the average slip can be estimated by following Eq. (2) and it is 8.25 m. Then the seismic moment can be transformed magnitude M_w by (Hanks and Kanamori, 1979)

$$M_\text{w} = \left(\frac{\log M_0}{1.5}\right) - 10.73 \tag{3}$$

Therefore, the maximum possible earthquake is M_w 8.15 ($M_0 = 2.07 \times 10^{28}$).

2.2 Stochastic Slip Model

5   The rupture process of an earthquake is extremely complex. The seismic inversion results reveal the slip distribution of rupture is heterogeneous with temporal development. Using a simplified uniform slip distribution to simulate tsunami only captures the long-wavelength portion of the tsunami fields (Geist and Dmowska, 1999). In addition, the temporal description of the seismic rupture process can be ignored because the propagation velocity of the tsunami waves is substantially slower than the seismic rupture velocity (Dean and Dalrymple, 1991; Ma et al., 1991; Wang and Liu, 2006). Andrews (1980) showed that

10   static slip distribution is directly related to stress changes and the spectrum of slip distribution is proportional to k^{-2} decay in wavenumber domain:

$$\left|F_{s,t}\left[D_{x,y}\right]\right| \propto k^{-2} \tag{4}$$

$D_{x,y}$ is the slip distribution over a 2D lattice, $F_{s,t}$ is the 2D Fourier transform, $k = \sqrt{k_x^2 + k_y^2}$ is the radial wavenumber. k^{-2} power law illustrates slip distribution has self-similar characteristics and from the fractal perspective, this characteristic also

15   can be demonstrated (Tsai, 1997). Herrero and Bernard (1994) based on self-similar introducing the k-square model which leads to the ω-square model (Aki, 1967). The slip spectrum follows k^{-2} decay beyond the corner radial wavenumber, k_c, which is proportional to $1/L_\text{c}$. The L_c depends on characteristic rupture dimension (Geist, 2002).

The heterogeneous slip distribution is proportional to k^{-2} and is similar to a fractional Brownian motion as a stochastic process

20   (Tsai, 1997). The stochastic slip distribution can be described by convolution in Fourier domain,

$$D_{x,y} \propto F_{x,y}^{-1}\left[F_{s,t}\left[X_{x,y}\right] \times k^{-2}\right] \tag{5}$$

where $X_{x,y}$ is random variable for spatial distribution; moreover, it makes phase random. $F_{x,y}^{-1}$ is the inverse 2D Fourier transform. The random distribution, X, which is best described by a non-Gaussian distribution, especially by a Lèvy distribution, can be calculated by reversing Eq. (5) (Lavallée and Archuleta 2003; Lavallée et al., 2006). Lèvy distribution can be described

25   by 4 parameters α, β, γ and μ_L. as below:

$$\varphi(t) = \begin{cases} \exp\left(-\gamma^\alpha |t|^\alpha \left[1 + i\beta\, \text{sign}(t)\tan\frac{\pi\alpha}{2}(|\gamma t|^{1-\alpha} - 1)\right] + i\mu_L t\right), & \alpha \neq 1 \\ \exp\left(-\gamma |t|\left[1 + i\beta\frac{2}{\pi}\text{sign}(t)(\ln|t| + \ln\gamma)\right] + i\mu_L t\right) & , \quad \alpha = 1 \end{cases} \tag{6}$$

The parameter α, $0 < \alpha \leq 2$, affects the falloff rate of probability density function (PDF) for the tail. The parameter β, $-1 \leq \beta \leq 1$, controls the skewness of PDF. The parameter γ, $\gamma > 0$, controls the width of PDF. The parameter μ_L, $-\infty < \mu_\text{L} < \infty$, is related to the

location of PDF. Lèvy distribution is good to describe the distribution of random variable, *X*, from real earthquake events, which implies the slip distribution without self-similar characteristic has heavy tail behavior (Lavallée et al., 2006). From the experiments of generating stochastic slip distribution, the heavy tail behavior affects the intensity of extreme value (Lavallée and Archuleta 2003).

The stochastic slip distribution is generated by 2D spatial random distribution with convoluting self-similar characteristic beyond the corner radial wavenumber, constraining by rupture dimension, in wavenumber domain. In this study, the potential rupture fault is divided into 5×5 km^2 subfaults. The number of gird mesh is 24×14 which are along strike and dip respectively. The spatial random variable produced adopts Lèvy distribution (α=1.51, β=0.2, γ=28.3, μ_L=-0.9) which is the dip slip result from Lavallée et al (2006) as Figure 1a. In Lavallée et al. (2006), the slip distribution of Northridge earthquake had been divided into the dip slip and strike slip directions and calculated by inverse 2D stochastic model to obtain the values of the Lèvy PDF. The values of the Lèvy PDF are given over to dip slip. The Northridge earthquake is a thrust earthquake (Davis 1994) so that it roughly has similar mechanism with our scenario fault model. In addition, the inversed slip distribution in study region is lack to do the analysis of Lèvy PDF. Therefore, the value of Lèvy distribution in Lavallée et al. (2006) is adopted in this study. In the perspective of mathematical operation, the slip distribution in Eq. (5) is a kind of filtered random distribution. However, for consistency with the physical behavior over the rupture surface supposed by the results of inverse method, the truncation has to be applied to the Lèvy distribution to constrain the extreme slip value. The synthetic slip distribution (Fig. 1b) produced by spatial random distribution in Figure 1a is heterogeneous and its power spectrum obeys *k*-square model at high wavenumber (Fig. 1c). The average slip of this synthetic slip distribution is 8.25 m, which represents earthquake energy keeping a constant as estimating above, and maximum slip is 31.02 m. The 100 different slip distributions are produced for tsunami simulation. They represent the uncertainty of results of complex rupture process. In 100 sets, the maximum slip range is between 20.17 to 37.97 m. There are no smooth process and extra regional constrain for slip distribution. There are two reasons for this application. The first is that we do not have information for where is locked or the location of asperity often repeats in historical event. The second is that there are some studies present the asperity expanding to the boundary of fault model (Ide et al., 2011; Lay et al., 2011; Shao et al., 2011; Yue and Lay, 2011). According to these, we do not prefer to apply any extra constraint for stochastic slip distributions. By same token, the uniform slip case is a complete uniform slip distribution. Figure 1b and 1d are the stochastic distribution of the scenario source models causing the maximum and minimum wave height at the recording station 26 (Hualien) (Fig. 2). Both patterns affecting the propagation will show at Sect. 3.1.

2.3 Numerical Tsunami Simulation

Figure 2 shows computational domain, recording stations and fault model. The potential rupture fault is divided into 5×5 km^2 subfaults, and the stochastic slip distribution model is applied to determine the amount of discrete slip on each subfault. Vertical

seafloor displacements caused by rupture slip are calculated using elastic dislocation theory (Okada, 1985). The Cornell Multigrid Coupled Tsunami Model (COMCOT) is used to perform the tsunami simulations. COMCOT is capable of efficiently studying the entire life-span of a tsunami, including its generation, propagation, runup and inundation (Wang 2009). It has been widely used in studying many historical tsunami events, such as 1960 Chilean tsunami (Liu et al., 1995), 1992 Flores Islands tsunami (Liu et al., 1995), 2003 Algeria tsunami (Wang and Liu, 2005), 2004 Indian Ocean tsunami (Wang and Liu, 2006, 2007), and 2006 Ping-Tung tsunami, Taiwan (Wu, et al., 2008; Chen, et al., 2008). COMCOT solves the linear or nonlinear shallow water equations for spherical or Cartesian coordinates using the finite difference method. With the flexible nested grid system, it can properly exhibit both efficiency and accuracy from the near-coastal region to the far-field region. Two grid layers are used to simulate the propagation of tsunamis. The Manning coefficient is 0.013 in this study to assume a sandy sea bottom (Wu, et al., 2008). The bathymetry adopted NOAA's (National Oceanic and Atmospheric Administration) open data which can be download from https://maps.ngdc.noaa.gov/viewers/wcs-client/ (Amante and Eakins, 2009). The resolution of the outer layer is 4 minutes for the solution of the linear shallow water equation, and the resolution of the inner layer is 1 minute for the solution of the nonlinear form of the shallow water equation. There are 30 recording stations which refer to the positions of tidal gauges maintained by the Central Weather Bureau (CWB) along the coasts of Taiwan and the outlying islands. The website of CWB presents the location of tide stations http://e-service.cwb.gov.tw/HistoryDataQuery/index.jsp and http://www.cwb.gov.tw/V7e/climate/marine_stat/tide.htm. These locations are shifted slightly to the node of grid in order to record accurately. Table 1 presents the locations of recording stations.

3 The effect of heterogeneous slip on the tsunamis

The stochastic slip model produces different slip distributions with the same fault geometry, average slip and a constant seismic moment. The model is used to describe the heterogeneous slip pattern of earthquake and to further examine its effect on the tsunamis occurring at the southernmost end of the Ryukyu subduction zone adjacent to Taiwan. According to the previous sections, the maximum possible earthquake is determined to be M_w 8.15 with 8.25 m average slip. Furthermore, the uniform slip distribution on the rupture plane is also used to simulate tsunami for discussing the different between uniform and heterogeneous slip on the tsunamis.

3.1 Initial water elevation and energy propagation

The static vertical displacement of the ocean floor is modelled using the elastic dislocation theory (Okada, 1985) and considered static slip distribution. The vertical seafloor displacement is used to be initial water level, and the horizontal component of the seabed is not included in the simulation. Figure 3a shows the initial water elevations produced by uniform

slip distribution and Figure 3b is its maximum free-surface elevation during the propagation. Figure 3c and 3e are the initial water elevations produced by stochastic slip distributions (Fig. 1b and 1d). The initial water elevation by uniform slip is simple and smooth, but for the stochastic slip models are more complex and more heterogeneous. Nonuniform slip causes an apparent change in the wavelength distribution of the initial free-surface elevation (the potential energy distribution), which affects the path of energy propagation. In the uniform slip scenario, the maximum free-surface elevation pattern is clear and controlled by topography. However, many strong and seemingly chaotic paths of wave energy appear in the nonuniform scenarios, and the ocean surface field has more uncertainties in terms of flow. In Figure 3b, the maximum free-surface elevation mainly travels toward two places where the seafloor elevation becomes shallower, relative to the deep areas northeast of Taiwan as bathymetry in Fig. 2. Although the propagation by nonuniform slip distributions (Fig. 3d and 3f) also has the same characteristics, it is notable that the paths followed by the wave energy differ, which depends on the rupture pattern. At the northeast of Taiwan in Figure 3f, there is a strong wave path connecting the two higher elevation part. However, this behavior does not occur in Figure 3b and 3d. Besides that, at the footwall side, the maximum elevation of Figure 3d is higher than Figure 3f. In Figure 3b, the high elevation only appears along the coast at footwall side. These results indicate the wave energy variation depends on rupture pattern causing differences in wave paths and leads to totally different tsunami amplitudes.

3.2 Wave characteristic

There are 30 stations along the coasts for recording the motion of sea level. Relative to other stations, the station 25 (Shihti), 26 (Hualien) and 27 (Suao) are near the potential rupture fault, and they have high wave amplitude and enormous variation in the tsunami simulation of 100 different slip distributions so that the time series of wave heights at these stations are shown as an example (Fig. 4). The varied wavelength distribution of the initial free-surface elevation results in substantial phase changes and different wave heights. It's worth noting that the average of the disordered and chaotic time series produced by the 100 different slip distributions is almost identical to the results from the uniform case. This implies the uniform case simply represents an average result and it cannot represent all of the possible situations.

According to the statistical results from 100 different slip patterns (Table 1) for 30 stations, Hualien station has the maximum wave amplitude, 7.32 m, and its maximum wave amplitude interval is 1.87 to 7.32 m. It is the widest interval for any recording site and the standard deviation of this distribution is 1.024. These indicate that Hualien station has high uncertainty in this scenario setting. However, the maximum wave amplitudes from uniform slip are relatively lower than stochastic results. Following above lecture, we need to rethink about that the estimation of uniform slip case is available for hazard analysis or not, even only focusing on the maximum wave amplitude issue.

3.3 The peak tsunami amplitude probability

According to the results of our simulations, we calculated the probability of the peak/maximum tsunami amplitudes (PTA) at each recording station as shown in Figure 5 by histogram. In order to verify the representativeness of the PTA probability distributions, another 100 sets of different slip distributions had been produced with same seismic conditions and simulated.

5 In Figure 5, the shapes of PTA distributions from another 100 sets, black lines, are similar to the histograms, the first 100 sets. This results verify the representativeness of the PTA probability distributions in 100 sets. This test also reinforces the reproducibility of our simulations and demonstrates that the number of simulations is roughly satisfactory for statistical analysis. Of course, the more slip distribution we use, the more comprehensive and stable the range we obtain.

10 In Figure 5, the PTA distributions at eastern Taiwan, red markers, are obviously higher than the western, blue markers, due to the specified location of the source of tsunami. The shapes of PTA distributions at eastern Taiwan seem like log-normal distribution and at western, they seem like normal distribution. We suppose that the attenuation of wave propagation causes the shape of log-normal distribution degenerating into normal distribution. The PTA produced by uniform slip are generally located in the middle of the PTA distributions. Both of the PTA values from uniform slip distribution and the values of the

15 PTA from stochastic slip distribution models decrease with the distance from potential fault because of the attenuation of wave propagation (Fig. 5 is for all stations and Fig. 6 shows station 20 to 30 in the eastern Taiwan). However, some stations are not perfectly following this, for instance, station 17, 19 and 21 which could be affected by coastal topography and energy channel. From Figure 3d, station 21 comparing with neighboring coast is exactly at the location where the energy gathers. In addition, the broad distributions frequently occur at promontories along the coastline and are caused by complex propagation path effects

20 between the source region and the recording locations (Geist, 2002). There are many compound factors to affect the tsunami propagation and maximum wave height. Figure 6 presents the relation between distance and wave height and also shows the PTA distribution as Figure 5. The distance is the shortest between the stations and fault plane. On the footwall side, the station 20 and 22 are outer island. They do not face the energy path directly (Fig. 3f) so that the PTA distributions are lower than station 21 and 23; even though the distance from fault are similar. On the hanging wall, station 29 is far from coast comparing

25 other stations because of real location of station and numerical grid setting so that the PTA distribution is lower than station 30 (Fig. 3b). The PTA distributions and their average values roughly appear a linear decrease with distance except the near field, station 26 and 27. Moreover, the ranges of PTA distributions convergent with distance, too. On the other hand, the near field, station 26 and 27, are directly affected by seafloor deformation so that the PTA by uniform slip are quite low.

30 Although the seismic parameters have defined already in our experiment and been held constants, there exist an uncertainty for PTA rather than a constant value. The uniform case cannot provide it and the PTA could be underestimated. Results give specific PTA ranges, which are the wave height uncertainties for the scenario of the earthquakes from Ryukyu Trench. It is necessary to consider the effect by heterogeneous slip distribution for a comprehensively assessing tsunami hazard.

4 Discussion

4.1 Tsunami

5 Most coast threatened by near-field tsunami is parallel the subduction zone like the coast of Chile, Japan and Indonesia. There are many tsunami event occurring these regions such as the 2010, Mw 8.8, Chile earthquake (Lay et al., 2010; Fritz et al., 2011), the 2011, Mw 9.0, Tohoku earthquake (Goda et al., 2015; Goda and Song, 2016), the 2004, Mw 9.1, Sumatra earthquake (Lay et al., 2005), and the 2010, Mw 8.1, Mentawai earthquake (Satake et al., 2013). However, the potential rupture fault in this study along the southernmost Ryukyu subduction zone is perpendicular to the coast of Taiwan island, which directly

10 affects the first movement of wave. On the footwall, the first movement is up, but conversely, it is down. On the hanging wall, the coastline backs from land to sea at first tsunami wave that help people have more time to leave seafront.

The effect by heterogeneous slip is important and necessary to consider for the near field estimation (Geist, 2002 and Ruiz et al., 2015). Figure 5 shows that the PTA distributions in the near field are broad and narrow with distance increasing from

15 potential fault. The uncertainty in near field is higher than far field. At the most of east stations, the values of average PTA approach uniform results, but at station 25 and 26, their uniform slip results are close to minimum PTA (Table 1.). Geist (2002) presents average and extrema PTA in nearshore calculated for 100 different slip distributions and compares with uniform slip result (Figure 6a in Geist, (2002)). The range of PTA also narrows with distance increasing. The values of uniform slip result and average of PTA are similar, but there are some average values close to minimum PTA around 19°N to 19.5°N. There is

20 similar characteristic of average PTA and uniform results in different region. The average PTA is equal to uniform slip result in nearshore, that could be caused by the factors (e.g. distance to the tsunami source, propagation path, etc.) to affect the average PTA to close to minimum PTA.

There are four nuclear power plants (NPP) on the Taiwan island. According to the numerical results, we infer that the PTA

25 mean value of NPP4 coastal area is around 2 to 3 m. This distribution may be wilder than other nuclear power plants due to the relative position of tsunami source. Moreover, NPP4 locates a bay with curved shape so that the extra magnification effect perhaps makes PTA higher. The NPP3 also has this condition and then the energy concentrates at this area (Fig 3b, 3d and 3f). For NPP1 and NPP2 coastal area, the PTA distributions are between 1 and 2 m. The coast of this two nuclear power plants is facing the tsunami current slightly so that its PTA should be higher than neighbor coast (Fig 3b, 3d and 3f). In general, under

30 this scenario, the coast of NPP4 has largest threat. Although the NPP3 is far from this tsunami source, it roughly faces 1.5 m wave height on average and has ±0.5m uncertain range. However, the NPP3 is more close to Manila subduction zone which

could be threatened by the tsunami from Manila Trench. The coast of NPP1 and NPP2 is relative safe and has less uncertainty for PTA.

The use of a heterogeneous slip pattern clearly delineates the range of possible waveforms and provides more information on latent uncertainties of wave height. The 95% confidence intervals for wave height from 100 sets present in each time series and provide us a specific range for the motion of sea level (Fig. 4). According to these time series, we are aware of the periods of tsunami runup and runoff and can prepare the supporting policies to reduce disaster. For example, a nuclear power plant has the trench of water intake from ocean for cooling reactor, and if the motion of sea level is too low to take the water, the temperature of reactor will be too high and then cause the nuclear disaster. This issue is necessary to pay attention in Taiwan because there are four unclear power plants located near the coast.

4.2 Stochastic slip model

The results of tsunami simulations illustrate that the effect of the slip distribution on the rupture plane has a significant effect on wave propagation and wave height. The correctness of this slip distribution determines whether the wave height calculations represent a useful reference or not. However, some parameters of stochastic model could influence synthetic slip distributions. For instance, the exponent of slip spectrum associates with roughness of slip distribution. Higher exponential value inhibits the power of high wavenumber and leads it smoother; conversely, lower value leads it rougher. In general, k-square model needs to be followed. Furthermore, interpolation of slip distribution for a given geometry will affect the exponent of k (Tsai, 1997). Interpolation make original pattern smoother. The short wavenumber will be depressing and the long wavenumber will be enhancing. Additionally, the random spatial variability of the slip distribution is more critical. According to Lavallée and Archuleta (2003) and Lavallée et al., (2006), we adopted the truncated non-Gaussian distribution as a spatial variability. Truncation limits the non-Gaussian distribution to a particular range. The extreme truncation will cause the heavy-tailed characteristic of this distribution to become less pronounced or even disappear, as in a Gaussian distribution. The synthetic slip is a filtering process in mathematics so that the heavy-tailed characteristic affects the extremum of slip distribution. The maximum slip will be greater as the truncated range increases. The maximum slip may exceed reasonable values as truncated range is too wide. Therefore, the parameters must be chosen carefully in order to match the observations acquired by inversion.

5 Conclusion

The maximum possible earthquake scenario is M_w 8.15 with average slip of 8.25 m in the southernmost portion of the Ryukyu Trench. The 100 slip distributions of the seismic rupture surface were generated by a stochastic slip model. The maximum slip range is between 20.17 to 37.97 m and the average slip all consists with 8.25 m. The heterogeneous slip induces variability in

tsunami wave heights and the associated paths of propagation. The simulated results demonstrate that rupture complexity has a significant influence on the near field for local tsunami. The PTA distribution provide a specific range for wave height and its occurring probability in this scenario. These distributions and their average values roughly appear a linear decrease with distance. The coast, which is very close tsunami source or even upon, is directly affected by rupture slip. Then, the range of

5   PTA distribution will converge with distance increasing from tsunami source. In this study, Hualien station, which is upon the source, has the wildest PTA interval (1.87-7.32 m) and the highest wave amplitude. The statistical summary reveals this station, whose standard deviation is 1.63 and larger than other stations, has the largest uncertainty. However, the PTA caused by the uniform slip distribution is only 1.63 m, which is much lower, even below average (3.36 m) in this station. It implies that a simplified earthquake source cannot completely represent tsunami amplitudes in reality. If we adopt uniform slip to assess

10   tsunami hazard, it will be critically underestimated. The tsunami amplitudes, which have characteristically extreme variance, are imperative for assessing tsunami hazards and the quantitative techniques is also important.

References

Aki, K.: Scaling law of seismic spectrum, J. Geophys. Res., 72, 1217-1231, 1967. doi:10.1029/JZ072i004p01217

15   Amante, C. and Eakins, B. W.: ETOPO1 1 arc-minute global relief model: procedures, data sources and analysis, US Department of Commerce, National Oceanic and Atmospheric Administration, National Environmental Satellite, Data, and Information Service, National Geophysical Data Center, Marine Geology and Geophysics Division Colorado, 2009. doi:10.7289/V5C8276M

Andrews, D. J.: A stochastic fault model: 1. Static case, J. Geophys. Res. Solid Earth, 85, 3867-3877, 1980.

20   doi:10.1029/JB085iB07p03867

Burroughs, S. M. and Tebbens, S. F.: Power-law scaling and probabilistic forecasting of tsunami runup heights, Pure Appl. Geophys., 162, 331-342, 2005. doi:10.1007/s00024-004-2603-5

Chen, P.-F., Newman, A. V., Wu, T.-R., and Lin, C.-C.: Earthquake Probabilities and Energy Characteristics of Seismicity Offshore Southwest Taiwan, Terr. Atmos. Ocean. Sci., 19, 2008. doi:10.3319/TAO.2008.19.6.697(PT)

25   Cheng, S.-N., Shaw, C.-F., and Yeh, Y. T.: Reconstructing the 1867 Keelung Earthquake and Tsunami Based on Historical Documents, Terr. Atmos. Ocean. Sci., 27, 2016. doi:10.3319/TAO.2016.03.18.01(TEM)

Cornell, C. A.: Engineering seismic risk analysis, Bull. Seism. Soc. Am., 58, 1583-1606, 1968.

Davis, T. L. and Namson, J. S.: A Balanced Cross-Section of the 1994 Northridge Earthquake, Southern California, Nature, 372, 167-169, 1994. doi:10.1038/372167a0

30   Dean, R. G. and Dalrymple, R. A.: Water wave mechanics for engineers and scientists, World Scientific Publishing Co Inc, 1991. doi:10.1142/9789812385512_0004

Fowler, C. M. R.: The Solid Earth: An Introduction to Global Geophysics, Cambridge University Press, Cambridge. pp. 728. 2004. ISBN-10: 0521893070

Fritz, H. M., Petroff, C. M., Catalán, P. A., Cienfuegos, R., Winckler, P., Kalligeris, N., Weiss, R., Barrientos, S. E., Meneses, G., Valderas-Bermejo, C., Ebeling, C., Papadopoulos, A., Contreras, M., Almar, R., Dominguez, J. C., and Synolakis, C. E.: Field Survey of the 27 February 2010 Chile Tsunami, Pure Appl. Geophys., 168, 1989-2010, 2011. doi:10.1007/s00024-011-0283-5

Geist, E. L.: Complex earthquake rupture and local tsunamis, J. Geophys. Res. Solid Earth, 107, ESE 2-1-ESE 2-15, 2002. doi:10.1029/2000JB000139

Geist, E. L. and Dmowska, R.: Local Tsunamis and Distributed Slip at the Source. In: Seismogenic and Tsunamigenic Processes in Shallow Subduction Zones, Sauber, J. and Dmowska, R. (Eds.), Birkhäuser Basel, Basel, 1999. doi:10.1007/978-3-0348-8679-6_6

Geist, E. L. and Parsons, T.: Probabilistic Analysis of Tsunami Hazards*, Nat. Hazards, 37, 277-314, 2006. doi:10.1007/s11069-005-4646-z

Geist, E. L. and Parsons, T.: Assessment of source probabilities for potential tsunamis affecting the U.S. Atlantic coast, Mar. Geol., 264, 98-108, 2009. doi:10.1016/j.margeo.2008.08.005

Goda, K. and Song, J.: Uncertainty modeling and visualization for tsunami hazard and risk mapping: a case study for the 2011 Tohoku earthquake, Stoch Environ Res Risk Assess, 30, 2271-2285, 2016. doi:10.1007/s00477-015-1146-x

Goda, K., Yasuda, T., Mori, N., and Mai, P. M.: Variability of tsunami inundation footprints considering stochastic scenarios based on a single rupture model: Application to the 2011 Tohoku earthquake, J. Geophys. Res. Oceans, 120, 4552-4575, 2015. doi:10.1002/2014JC010626

Gutenberg, B. and Richter, C. F.: Frequency of earthquakes in California, Bull. Seism. Soc. Am., 34, 185-188, 1944.

Hanks, T. C. and Kanamori, H.: A moment magnitude scale, J. Geophys. Res. Solid Earth, 84, 2348-2350, 1979. doi:10.1029/JB084iB05p02348

Herrero, A. and Bernard, P.: A Kinematic Self-Similar Rupture Process for Earthquakes, Bull. Seism. Soc. Am., 84, 1216-1228, 1994.

Horikawa, K. and Shuto, N.: Tsunami disasters and protection measures in Japan, Tsunamis-Their Science and Engineering, Terra Scientific Publishing Company, 1983. 9-22, 1983.

Houston, J. R., Carver, R. D., and Markle, D. G.: Tsunami-Wave Elevation Frequency of Occurrence for the Hawaiian Islands, Army Engineer Waterways Experiment Station, Vicksburg, MS, 66 pp, 1977.

Hsu, Y.-J., Ando, M., Yu, S.-B., and Simons, M.: The potential for a great earthquake along the southernmost Ryukyu subduction zone, Geophys. Res. Lett., 39, n/a-n/a, 2012. doi:10.1029/2012GL052764

Hsu, Y.-J., Yu, S.-B., Simons, M., Kuo, L.-C., and Chen, H.-Y.: Interseismic crustal deformation in the Taiwan plate boundary zone revealed by GPS observations, seismicity, and earthquake focal mechanisms, Tectonophysics, 479, 4-18, 2009. doi:10.1016/j.tecto.2008.11.016
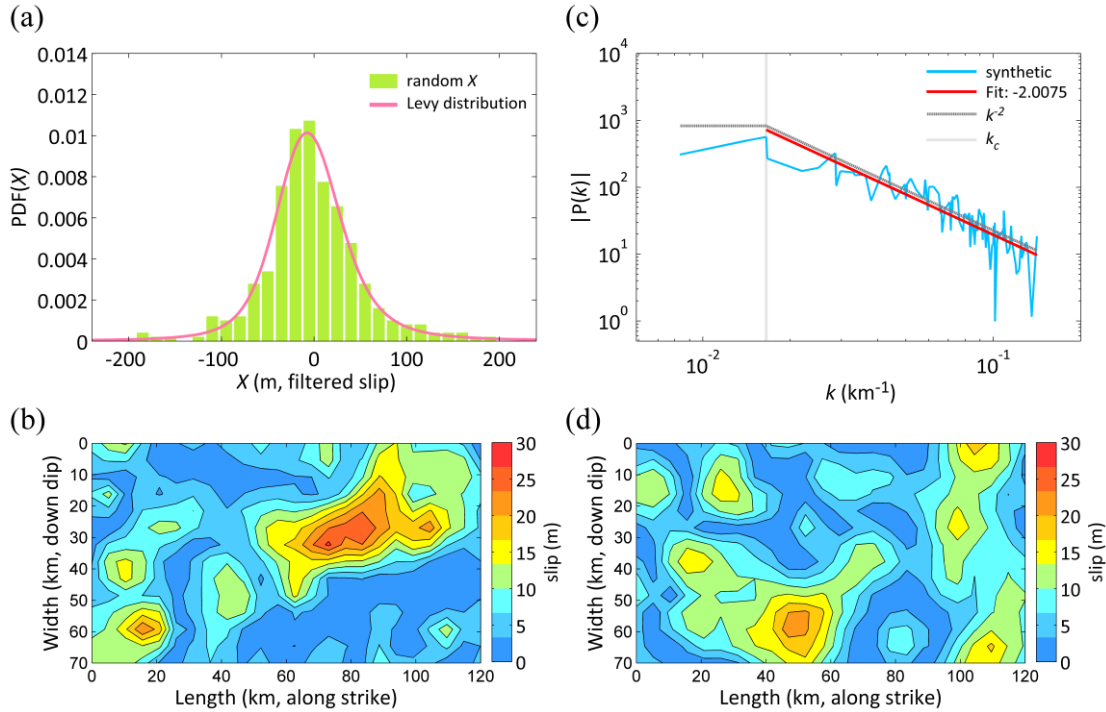
Ide, S., Baltay, A., and Beroza, G. C.: Shallow dynamic overshoot and energetic deep rupture in the 2011 Mw 9.0 Tohoku-Oki earthquake, Science, 332, 1426-1429, 2011. doi:10.1126/science.1207020

Kanamori, H. and Anderson, D. L.: Theoretical basis of some empirical relations in seismology, Bull. Seism. Soc. Am., 65, 1073-1095, 1975.

5 Lavallée, D. and Archuleta, R. J.: Stochastic modeling of slip spatial complexities for the 1979 Imperial Valley, California, earthquake, Geophys. Res. Lett., 30, 1245, 2003. doi:10.1029/2002GL015839

Lavallée, D., Liu, P., and Archuleta, R. J.: Stochastic model of heterogeneity in earthquake slip spatial distributions, Geophys. J. Int., 165, 622-640, 2006. doi:10.1111/j.1365-246X.2006.02943.x

Lay, T., Ammon, C. J., Kanamori, H., Koper, K. D., Sufri, O., and Hutko, A. R.: Teleseismic inversion for rupture process of

10 the 27 February 2010 Chile (Mw 8.8) earthquake, Geophys. Res. Lett., 37, L13301, 2010. doi:10.1029/2010GL043379

Lay, T., Ammon, C. J., Kanamori, H., Xue, L., and Kim, M. J.: Possible large near-trench slip during the 2011 Mw 9.0 off the Pacific coast of Tohoku Earthquake, Earth Planets Space, 63, 32, 2011. doi:10.5047/eps.2011.05.033

Lay, T., Kanamori, H., Ammon, C. J., Nettles, M., Ward, S. N., Aster, R. C., Beck, S. L., Bilek, S. L., Brudzinski, M. R., Butler, R., DeShon, H. R., Ekström, G., Satake, K., and Sipkin, S.: The Great Sumatra-Andaman Earthquake of 26 December

15 2004, Science, 308, 1127-1133, 2005. doi:10.1126/science.1112250

Lay, T. and Wallace, T. C.: Modern global seismology, Academic press, 1995. ISBN: 9780127328706

Liu, P. L. F., Cho, Y. S., Yoon, S. B., and Seo, S. N.: Numerical Simulations of the 1960 Chilean Tsunami Propagation and Inundation at Hilo, Hawaii. In: Tsunami: Progress in Prediction, Disaster Prevention and Warning, Tsuchiya, Y. and Shuto, N. (Eds.), Springer Netherlands, Dordrecht, 1995. doi:10.1007/978-94-015-8565-1_7

20 Liu, P. L. F., Cho, Y. S., Briggs, M. J., Kanoglu, U., and Synolakis, C. E.: Runup of solitary waves on a circular Island, J. Fluid Mech., 302, 259-285, 1995. doi:10.1017/S0022112095004095

Ma, K.-F. and Lee, M.-F.: Simulation of historical tsunamis in the Taiwan region, Terr. Atmos. Ocean. Sci., 8, 13-30, 1997.

Ma, K.-F., Satake, K., and Kanamori, H.: The origin of the tsunami excited by the 1989 Loma Prieta Earthquake —Faulting or slumping?, Geophys. Res. Lett., 18, 637-640, 1991. doi:10.1029/91GL00818

25 Mimura, N., Yasuhara, K., Kawagoe, S., Yokoki, H., and Kazama, S.: Damage from the Great East Japan Earthquake and Tsunami - A quick report, Mitig Adapt Strat Gl, 16, 803-818, 2011. doi:10.1007/s11027-011-9297-7

Nakamura, M.: Fault model of the 1771 Yaeyama earthquake along the Ryukyu Trench estimated from the devastating tsunami, Geophys. Res. Lett., 36, n/a-n/a, 2009. doi:10.1029/2009GL039730

Okada, Y.: Surface deformation due to shear and tensile faults in a half-space, Bull. Seism. Soc. Am., 75, 1135-1154, 1985.

30 Okal, E. A.: Mode-wave equivalence and other asymptotic problems in tsunami theory, Phys. Earth Planet. Inter., 30, 1-11, 1982. doi:10.1016/0031-9201(82)90123-6

Piombo, A., Tallarico, A., and Dragoni, M.: Displacement, strain and stress fields due to shear and tensile dislocations in a viscoelastic half-space, Geophys. J. Int., 170, 1399-1417, 2007. doi:10.1111/j.1365-246X.2007.03283.x

Ruiz, J. A., Fuentes, M., Riquelme, S., Campos, J., and Cisternas, A.: Numerical simulation of tsunami runup in northern Chile based on non-uniform k−2 slip distributions, Nat. Hazards, 79, 1177-1198, 2015. doi:10.1007/s11069-015-1901-9

Satake, K., Nishimura, Y., Putra, P. S., Gusman, A. R., Sunendar, H., Fujii, Y., Tanioka, Y., Latief, H., and Yulianto, E.: Tsunami Source of the 2010 Mentawai, Indonesia Earthquake Inferred from Tsunami Field Survey and Waveform Modeling,

5   Pure Appl. Geophys., 170, 1567-1582, 2013. doi:10.1007/s00024-012-0536-y

Sella, G. F., Dixon, T. H., and Mao, A.: REVEL: A model for Recent plate velocities from space geodesy, J. Geophys. Res. Solid Earth, 107, ETG 11-11-ETG 11-30, 2002. doi:10.1029/2000JB000033

Senior Seismic Hazard Analysis Committee (SSHAC): Recommendations for probabilistic seismic hazard analysis: guidance on uncertainty and use of experts, US Nuclear Regulatory Commission Washington, DC, 1997. doi:10.2172/479072

10   Seno, T., Stein, S., and Gripp, A. E.: A model for the motion of the Philippine Sea Plate consistent with NUVEL-1 and geological data, J. Geophys. Res. Solid Earth, 98, 17941-17948, 1993. doi:10.1029/93JB00782

Shao, G., Li, X., Ji, C., and Maeda, T.: Focal mechanism and slip history of the 2011 Mw 9.1 off the Pacific coast of Tohoku Earthquake, constrained with teleseismic body and surface waves, Earth Planets Space, 63, 9, 2011. doi:10.5047/eps.2011.06.028

15   Soloviev, S.: Recurrence of tsunamis in the Pacific, Tsunamis in the Pacific Ocean, 1970. 149-163, 1970.

Theunissen, T., Font, Y., Lallemand, S., and Liang, W.-T.: The largest instrumentally recorded earthquake in Taiwan: revised location and magnitude, and tectonic significance of the 1920 event, Geophys. J. Int., 183, 1119-1133, 2010. doi:10.1111/j.1365-246X.2010.04813.x

Tsai, C.-C. P.: Slip, Stress Drop and Ground Motion of Earthquakes: A View from the Perspective of Fractional Brownian

20   Motion, Pure Appl. Geophys., 149, 689-706, 1997. doi:10.1007/s000240050047

Tsai, Y.-B.: A study of disastrous earthquakes in Taiwan, 1683−1895, Bull. Inst. Earth Sci., Acad. Sin. 5, 1-44, 1985

Wang, X.: User manual for COMCOT version 1.7 (first draft). Cornel University, 65., 2009.

Wang, X. M. and Liu, P. L. F.: A numerical investigation of Boumerdes-Zemmouri (Algeria) earthquake and tsunami, CMES Comput. Model. Eng. Sci., 10, 171-183, 2005. doi:10.3970/cmes.2005.010.171

25   Wang, X. and Liu, P. L. F.: An analysis of 2004 Sumatra earthquake fault plane mechanisms and Indian Ocean tsunami, J. Hydraul. Res., 44, 147-154, 2006. doi:10.1080/00221686.2006.9521671

Wang, X. and Liu, P. L. F.: Numerical simulations of the 2004 Indian Ocean tsunamis — coastal effects, J. Earthquake and Tsunami, 01, 273-297, 2007. doi:10.1142/s179343110700016x

Wang, Y.-J., Chan, C.-H., Lee, Y.-T., Ma, K.-F., Shyu, J., Rau, R.-J., and Cheng, C.-T.: Probabilistic seismic hazard

30   assessment for Taiwan, Terr. Atmos. Ocean. Sci., 27, 2016. doi:10.3319/TAO.2016.05.03.01(TEM)

Wu, T.-R., Chen, P.-F., Tsai, W.-T., and Chen, G.-Y.: Numerical Study on Tsunamis Excited by 2006 Pingtung Earthquake Doublet, Terr. Atmos. Ocean. Sci., 19, 705-715, 2008. doi:10.3319/TAO.2008.19.6.705(PT)

Wu, Y.-H., Chen, C.-C., Turcotte, D. L., and Rundle, J. B.: Quantifying the seismicity on Taiwan, Geophys. J. Int., 194, 465-469, 2013. doi:10.1093/gji/ggt101

Yu, N.-T., Yen, J.-Y., Chen, W.-S., Yen, I. C., and Liu, J.-H.: Geological records of western Pacific tsunamis in northern Taiwan: AD 1867 and earlier event deposits, Mar. Geol., 372, 1-16, 2016. doi:10.1016/j.margeo.2015.11.010

Yu, S.-B., Chen, H.-Y., and Kuo, L.-C.: Velocity field of GPS stations in the Taiwan area, Tectonophysics, 274, 41-59, 1997. doi:10.1016/S0040-1951(96)00297-1

5   Yue, H. and Lay, T.: Inversion of high-rate (1 sps) GPS data for rupture process of the 11 March 2011 Tohoku earthquake (Mw 9.1), Geophys. Res. Lett., 38, L00G09, 2011. doi:10.1029/2011GL048700

Fig. 1. (a) The spatial random variable: truncated Lèvy distribution. Lèvy parameters obtained from the Northridge earthquake were taken from Lavallée et al (2006). (b) A stochastic slip is generated from filtering the spatial random variable _X_, Fig. 1a. This slip pattern produces the highest maximum wave amplitude at Hualien station. (c) Slip spectrum is calculated from Fig. 1b. This slip spectrum decays with exponent of -2 and characteristic of corner radial wavenumber. It verifies that synthetic slip is identical with k-square model and condition of rupture dimension. (d) This stochastic slip distribution produces the lowest maximum wave amplitude at Hualien station.
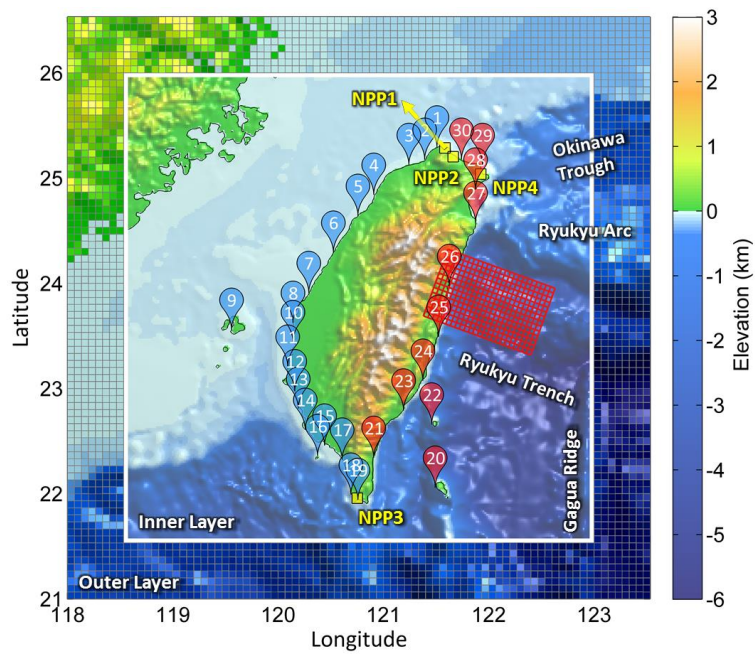
Fig. 2. The map of Taiwan presents the fault model and recoding stations used in this study. The bathymetry is divided into 2 layer for different resolutions. The resolution of the outer layer is 4 minutes, and the resolution of the inner layer of the white box is 1 minute. The red grid denotes the potential fault model (5×5 km^2). Pins represent 30 tidal gauges of the CWB. The red and blue colors indicate stations on the east and west sides of Taiwan respectively. Yellow squares represent the sites of the nuclear power plants.
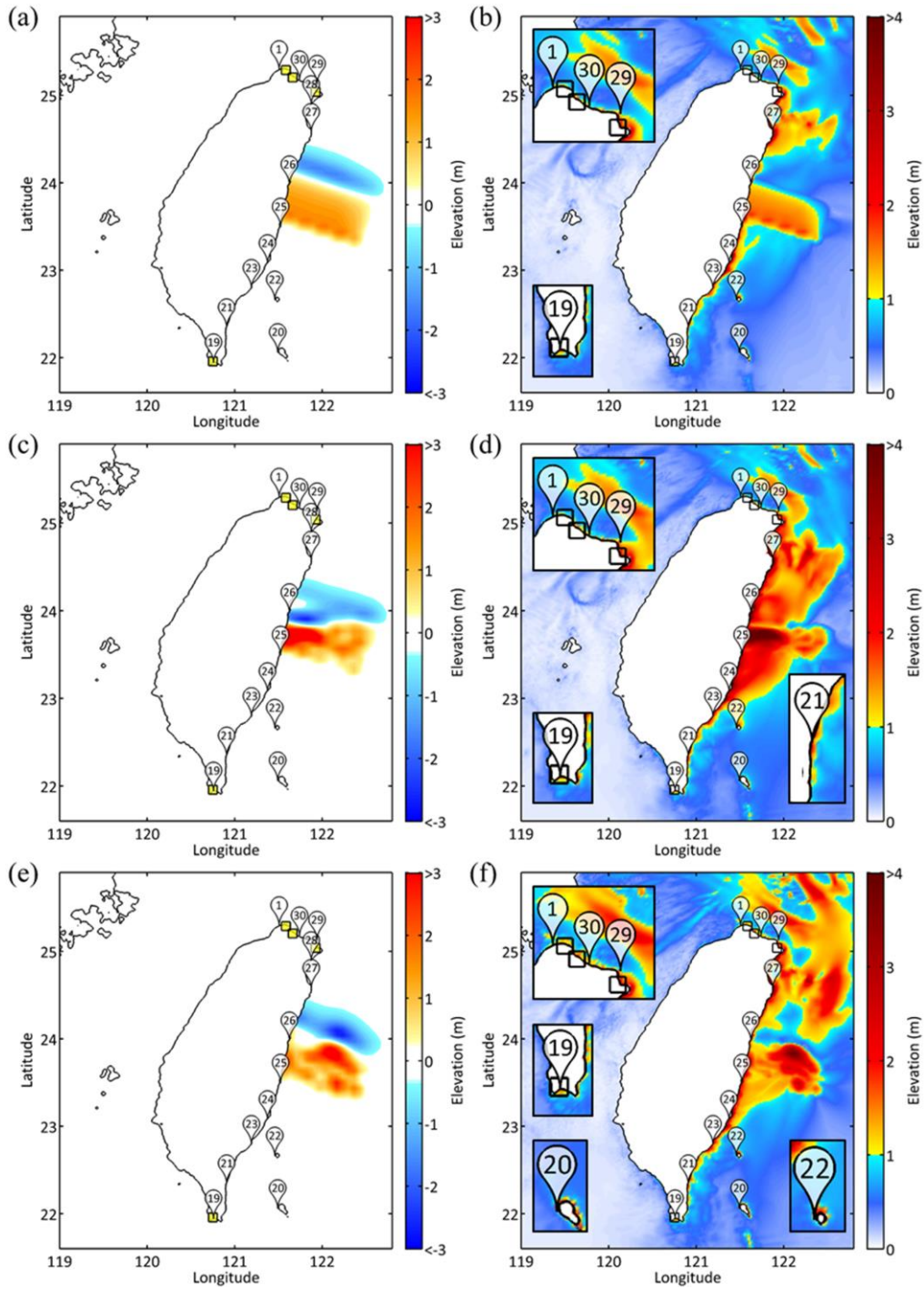
5

Fig. 3. (a), (c) and (e) are the initial water elevation and colorbar represents the elevation of initial water surface. (b), (d) and (f) are maximum free-surface elevation, the distribution of energy path, and colorbar represents the elevation of maximum free-surface. (a) and (b) displays the results from uniform slip distribution. (c) and (d) displays the results from Fig. 1b. (e) and (f) displays the results

from Fig. 1d. In fundamental, seafloor dominants tsunami propagation, but the slip distribution has strong influence. In (a, c and e), yellow squares represent nuclear power plants; in (b, d and f), they are open squares.
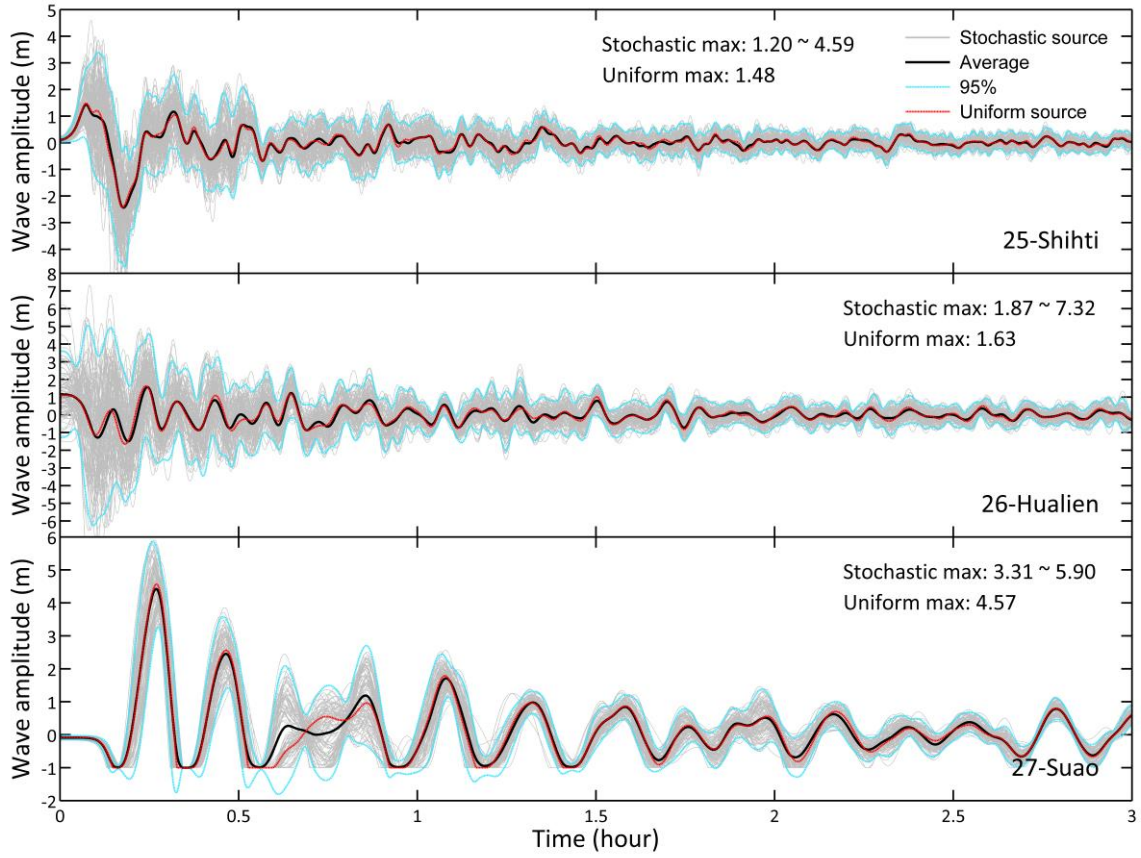
Fig. 4. The time series of wave heights recorded at station 25 (Shihti), 26 (Hualien) and 27 (Suao). Gray lines represent the time series of 100 different slip distributions; black lines represent the averages of the gray lines; blue lines represent the 95% confidence intervals; and red lines are the time series produced using uniform slip distributions. Parts of the wave heights on station 27 are lower than water depths, and these curves have been truncated.

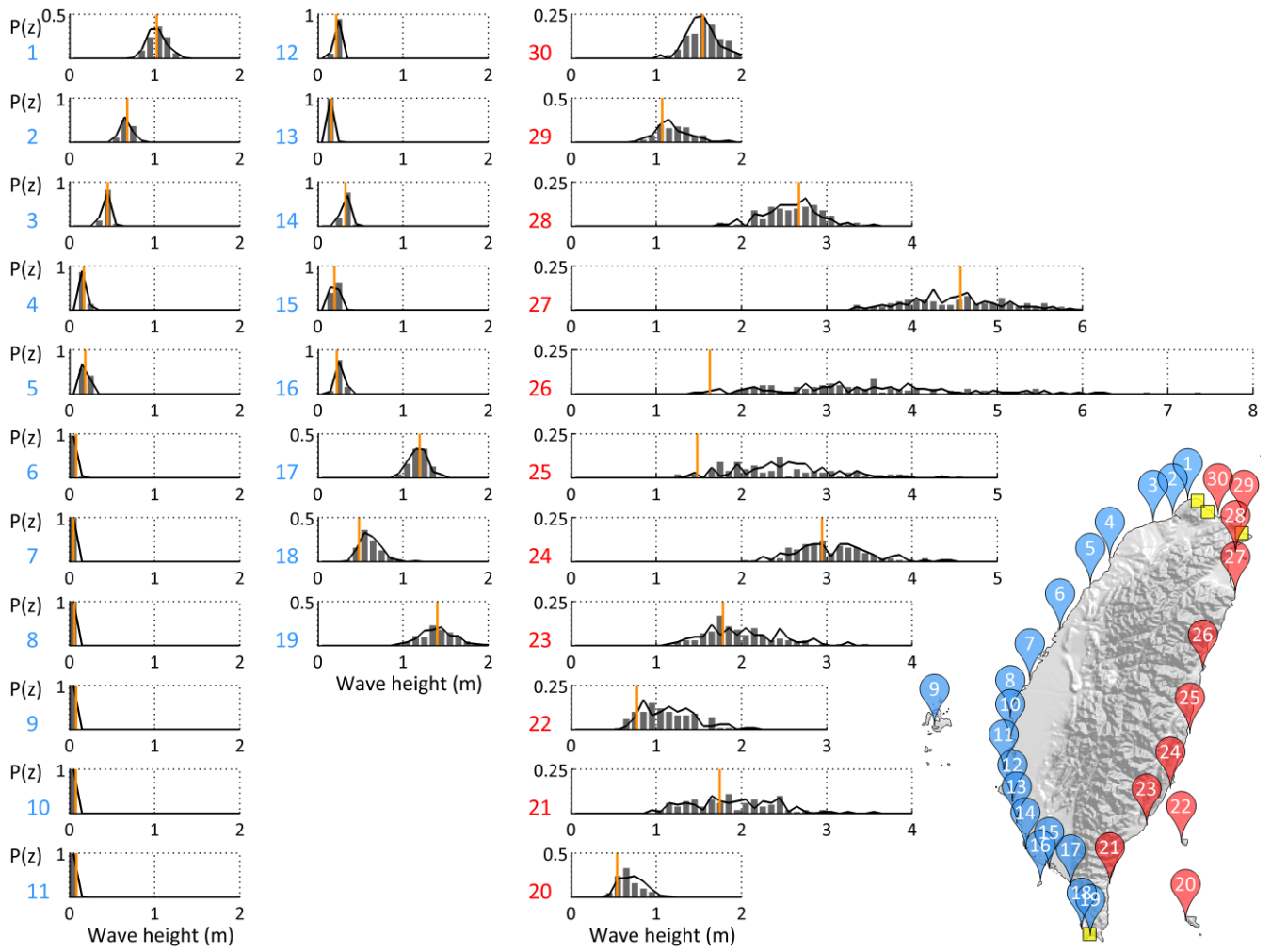**Fig. 5.** The probabilities of PTA along the coast of Taiwan (blue: 1~19, red: 20~30). The histograms display the PTA derived from 100 different slip simulations. The black lines represent the results from another 100 simulations, and the orange lines represent the PTA obtained using a uniform slip distribution. The PTA probability distribution give a clear PTA range and its occurring probability.
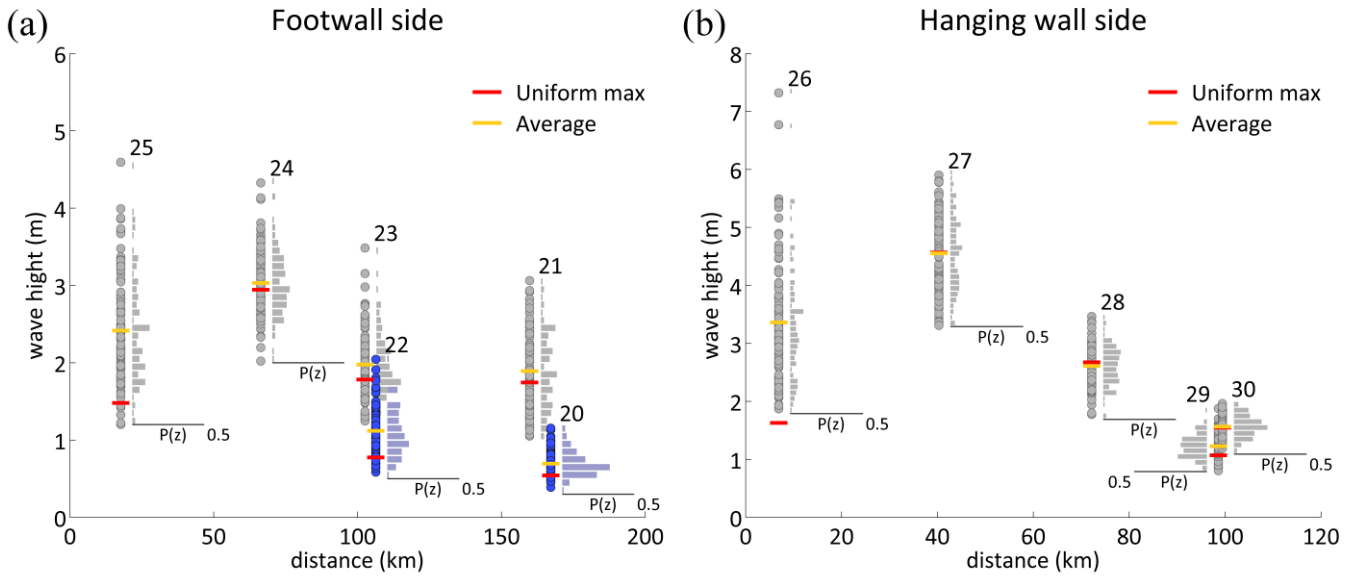
Fig. 6. The relation between distance and wave height for stations from 20 to 30 in the eastern Taiwan. (a) is the station on the footwall side. Station 20 and 22, blue color, are out of Taiwan island. (b) is the stations on the hanging wall side. Both sides roughly appear a linear decay and uncertainty range converging with distance increasing for tsunami amplitude. Red bars show the PTA of the uniform slip distribution and yellow bars show the average of the PTA from stochastic slip models.

Table 1. This table lists the maximum, minimum, standard deviation and average wave heights for the PTA probability distributions in meter. It also lists the maximum wave heights from uniform slip model.

#	Station	Lon.	Lat.	Min [m]	Max [m]	σ [m]	Avg. [m]	Max [m] (uniform slip)
1	Linshanbi	121.5106	25.2844	0.80	1.32	0.108	1.04	1.02
2	Danshuei	121.4019	25.1844	0.55	0.83	0.061	0.68	0.68
3	Jhuwei	121.2353	25.1200	0.33	0.52	0.039	0.44	0.45
4	Hsinchu	120.9122	24.8503	0.13	0.24	0.025	0.17	0.17
5	Waipu	120.7717	24.6514	0.15	0.26	0.020	0.20	0.19
6	Taichung Port	120.5250	24.2917	0.07	0.11	0.009	0.08	0.08
7	Fanyuan	120.2972	23.9147	0.04	0.06	0.004	0.05	0.05
8	Bozihliao	120.1417	23.6250	0.05	0.07	0.004	0.06	0.06
9	Penghu	119.5669	23.5636	0.07	0.09	0.005	0.08	0.08
10	Dongshih	120.1417	23.4417	0.06	0.09	0.005	0.08	0.08
11	Jiangjyun	120.1000	23.2181	0.06	0.10	0.007	0.09	0.09

20

12	Anping	120.1583	22.9750	0.15	0.26	0.018	0.22	0.22
13	Yongan	120.1917	22.8083	0.11	0.20	0.016	0.16	0.16
14	Kaohsiung	120.2883	22.6144	0.23	0.43	0.039	0.33	0.33
15	Donggang	120.4417	22.4583	0.15	0.28	0.026	0.21	0.20
16	Siaoliouciou	120.3750	22.3583	0.17	0.40	0.046	0.26	0.22
17	Jiahe	120.6083	22.3250	0.90	1.44	0.098	1.19	1.20
18	Syunguangzuei	120.6917	21.9917	0.33	0.96	0.124	0.61	0.49
19	Houbihu	120.7583	21.9417	0.90	1.96	0.197	1.41	1.40
20	Lanyu	121.4917	22.0583	0.39	1.15	0.155	0.69	0.54
21	Dawu	120.8972	22.3375	1.05	3.06	0.487	1.89	1.74
22	Lyudao	121.4647	22.6622	0.58	2.04	0.316	1.12	0.78
23	Fugang	121.1917	22.7917	1.25	3.48	0.409	1.98	1.78
24	Chenggong	121.3767	23.0889	2.02	4.33	0.416	3.03	2.94
25	Shihti	121.5250	23.4917	1.20	4.59	0.680	2.42	1.48
26	Hualien	121.6231	23.9803	1.87	7.32	1.024	3.36	1.63
27	Suao	121.8686	24.5856	3.31	5.90	0.641	4.55	4.57
28	Gengfang	121.8619	24.9072	1.78	3.47	0.337	2.61	2.67
29	Longdong	121.9417	25.1250	0.80	1.88	0.202	1.23	1.07
30	Keelung	121.7417	25.1750	1.19	1.96	0.183	1.57	1.55